Achromatic three-wave (or more) lateral shearing interferometer

J. Primot and L. Sogno

Office National d'Etudes et de Recherches Aérospatiales, BP 72, 92322 Châtillon Cedex, France

Received October 17, 1994; revised manuscript received June 20, 1995; accepted July 6, 1995

A new kind of lateral shearing interferometer, called the three-wave lateral shearing interferometer, was previously described [Appl. Opt. **32**, 6242 (1993)]. As this instrument was monochromatic and its usable light efficiency was poor, the proposed setup was well suited only for a class of wave-front sensing problems, such as optical testing, in which the source can be easily adapted. A new achromatic setup adapted to low light level applications is presented. Three replicas of the analyzed wave front are obtained by Fourier filtering of the orders diffracted by a microlens array. An important feature of these new devices is their great similarity to another class of wave-front sensors based on the Hartmann test.

Key words: interferometry, optical testing, adaptive optics, active optics, wave-front sensing, microlens array.

1. INTRODUCTION

Lateral shearing interferometers (LSI's) offer one a wide variety of optical arrangements in dealing with different wave-front sensing problems, such as optical testing, turbulence estimation, and active or adaptive optics control.[1–4] However, the usual setups are based on the interference of replicas of the analyzed wave front, translated laterally in one direction. The obtained intensity figure is then related to the phase gradient in the direction of the translation. These setups need to be spatially or temporally split to yield the two orthogonal gradients required for phase reconstruction.

In a previous paper we proposed to generalize this principle.[5] The interference pattern recorded in the three-wave lateral shearing interferometer (TWLSI) is now generated from three replicas of the analyzed wave front translated in noncollinear directions. The result is a fringe pattern related to the phase gradients in three directions. This working mode is detailed in Section 2. The three derived gradients are then used in the measurement of the two orthogonal phase gradients needed for reconstruction of the phase and estimation of the accuracy of the measured quantities. This is a substantial advantage, as it is of help in evaluating the accuracy of the reconstructed wave front.

However, the replication device that we suggested to obtain three replicas worked only with monochromatic light and had poor light efficiency. These two characteristics make it difficult to use for applications with low light level sources, such as adaptive or active optics control. The purpose of this paper is to design other replication devices that will avoid these major drawbacks. These new setups are not just a new version but a total revamping that leads one to a new way in which to consider TWLSI's. As will be seen below, it is a link between two widely used classes of wave-front sensors: LSI and Hartmann tests.

2. THREE-WAVE LATERAL SHEARING INTERFEROMETER: STATE OF THE ART

As the TWLSI is a generalization of the LSI class, producing biperiodic interferograms, it is obvious that it is possible to define many optical setups. The succeeding subsections will allow us to describe the essential features of TWLSI's and the state of the art, giving a starting point to the design of new devices for specific applications.

A. Three-Plane-Wave Interferograms

The TWLSI is essentially based on a remarkable optical property: the intensity figure related to the interference of three plane waves is independent of the longitudinal position on the considered propagation axis. This can be demonstrated by the geometrical construction shown in Fig. 1.

We plot three unit wave vectors $\mathbf{k}_1$, $\mathbf{k}_2$, $\mathbf{k}_3$ related to the three replicas, starting from one point of the replication plane. Their extremities belong to the same plane, which gives three points and thus defines a unique circle. The center of this circle, associated with the origin of the replication plane, defines a direction of propagation D_p such that the delays of the three plane waves are equal. The interference pattern is thus independent of the longitudinal position of an observation plane O_p perpendicular to this peculiar propagation axis. Now, if we consider another propagation axis D'_p associated with a new observation plane O'_p, the appearance of the interference pattern changes, as this new plane is not parallel to the previous one. However, the independence of the longitudinal position is obviously preserved.

As four or more points are rarely placed on the same circle, interference patterns for four or more plane waves do not behave the same way, except in special arrangements, which will be presented below.

0740-3232/95/122679-07$06.00

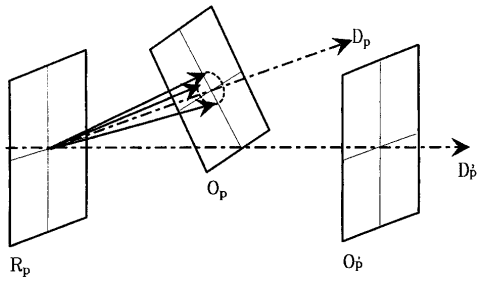

Fig. 1. Geometrical demonstration of the independence of the interference figure with respect to the longitudinal position of the observation plane.

B. Three-Wave Lateral Shearing Interferometer Conception

The TWLSI is essentially made up of two components. The first is a replication device. This divides the analyzed wave front into three replicas tilted with respect to three axes intercepting at 120° and lying in a common optical plane in which the analysis is to be made. Most of the time, this plane is the instrument pupil plane. The second component consists of a camera that can be translated longitudinally with respect to the propagation axis.

If the interference pattern of the three replicas is observed by the camera in the replication plane, the recorded image consists of a regular hexagonal array of bright spots, as shown in Fig. 2. If it is now observed in a distant plane, relative translations appear between the replicas, on account of the propagation of the tilted wave fronts, and the spots are displaced in the direction of the local phase gradients (Fig. 3). These displacements are proportional to the distance between the replication and observation planes. Thus the interferometer sensitivity is adjusted by an appropriate choice of the longitudinal position of the observation plane.

C. Replication Device

Although it is easy to split an optical beam into two equal parts, it is much harder to split it into three. The first design that we proposed consisted of a special optical arrangement of a separating cube and an optical flat.[5] As lateral shears were obtained by simple reflections on vitreous surfaces, they were independent of wavelength. So the pitch of the produced fringe pattern was dependent on the wavelength. The use of polychromatic light thus resulted in a global degradation of the interferogram contrast.

This setup provided a good balance among the three replicas and eliminated the weak additional replicas that lead to the superposition of parasitic fringe patterns. On the other hand, its light efficiency was very low, of the order of 1%, and it was exclusively devoted to monochromatic light applications.

Since we first designed this replication device, we have found other three-beam interferogram setups in the literature, especially in the field of optical techniques for generating microlens arrays.[6] However, as these devices are designed for another purpose, they are not all well suited for optical testing.

D. Phase Gradient Evaluation

The exact derivation of the phase gradients from the fringe pattern is beyond the scope of this paper and can be found in Ref. 5. However, we can summarize this process by saying that the interference pattern of the three replicas is made up of three couples of elementary interference patterns between two tilted and laterally shifted replicas. Fringe analysis consists in demodulating these superposed fringe patterns simultaneously.

In order to simplify the expressions, we do not include the local irradiance fluctuations of the analyzed wave front W in the following equations. Hence the complex amplitude is expressed as

$$A(\mathbf{x}) = \exp[iW(\mathbf{x})]. \tag{1}$$

The replication device generates three tilted replicas A_i:

$$A_i(\mathbf{x}) = \exp\{i[W(\mathbf{x}) + \mathbf{k}_i \cdot \mathbf{x}]\}, \tag{2}$$

where $\mathbf{k}_i$ is the wave vector of the tilted wave. The irradiance I_0 in the replication plane is then

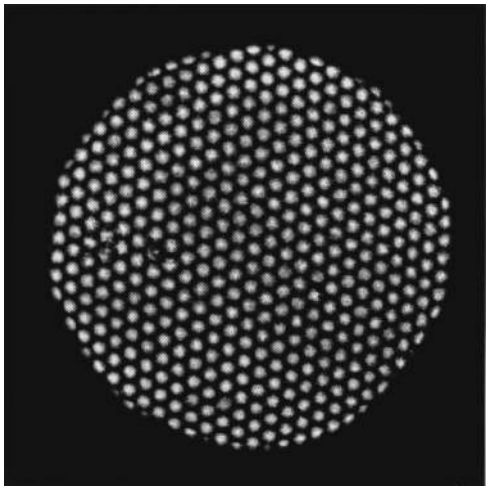

Fig. 2. Three-wave interferogram observed in the replication plane for a large spherical aberration.

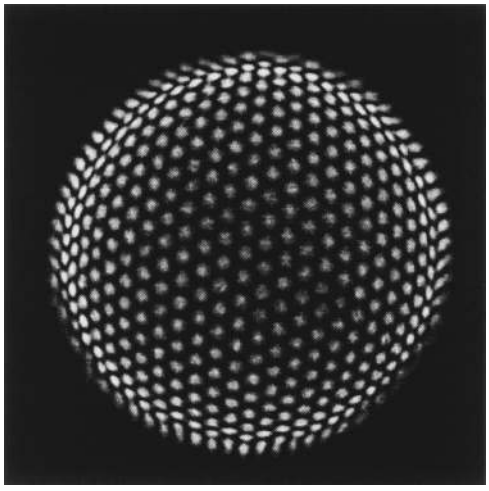

Fig. 3. Three-wave interferogram observed in a distant plane of the replication plane for a large spherical aberration. Note that the experimental setup is identical to that of Fig. 2 but for a longitudinal translation of the camera.

$$I_0(\mathbf{x}) = \left| \sum_{i=1}^{3} A_i(\mathbf{x}) \right|^2 = 3 + \sum_{i,j=1_{i\neq j}}^{3} \exp[i(\mathbf{k}_i - \mathbf{k}_j)\cdot\mathbf{x}]. \quad (3)$$

From the irradiance transport equation[7–9] the irradiance I_L obtained in a plane at a distance L is

$$I_L(\mathbf{x}) = I_0(\mathbf{x}) - \frac{L}{k}\left[\nabla I_0(\mathbf{x})\cdot\nabla W(\mathbf{x}) + I_0(\mathbf{x})\cdot\nabla^2 W(\mathbf{x})\right], \quad (4)$$

with k being the wave number. From the expression for I_0 this equation can be expanded to

$$I_L(\mathbf{x}) = 3\left[1 - \frac{L}{k}\nabla^2 W(\mathbf{x})\right] + \sum_{i,j=1_{i\neq j}}^{3}\left\{\left[1 - \frac{L}{k}\nabla^2 W(\mathbf{x})\right] - i\,\frac{L}{k}(\mathbf{k}_i - \mathbf{k}_j)\nabla W(\mathbf{x})\right\}\cdot\exp\left[i(\mathbf{k}_i - \mathbf{k}_j)\cdot\mathbf{x}\right]. \quad (5)$$

The Fourier transform of I_L is then

$$\mathrm{FT}(I_L)(\mathbf{u}) = 3\mathrm{FT}\left[1 - \frac{L}{k}\nabla^2 W(\mathbf{x})\right] + \sum_{i,j=1_{i\neq j}}^{3}\mathrm{FT}\left\{\left[1 - \frac{L}{k}\nabla^2 W(\mathbf{x})\right] - i\,\frac{L}{k}(\mathbf{k}_i - \mathbf{k}_j)\nabla W(\mathbf{x})\right\} * \delta\left[(\mathbf{k}_i - \mathbf{k}_j) - \mathbf{u}\right], \quad (6)$$

where $\mathbf{u}$ is a Fourier space vector associated with $\mathbf{x}$ and $*$ indicates convolution product.

This Fourier transform consists of a continuum plus six harmonics corresponding to the delta functions and placed at the vertices of a hexagon.

The first step in recovering the phase gradients in three directions separated by 120° consists in isolating three harmonics placed on one of the two isosceles triangles that can be defined in the hexagon. These three parts of the Fourier plane are then recentered one by one, and an inverse Fourier transform is performed. The complex quantities obtained are such that their imaginary part corresponds to the projection of the wave-front gradient $\nabla W(\mathbf{x})$ in the direction $(\mathbf{k}_i - \mathbf{k}_j)$ considered.

E. Advantages of a Three-Wave Lateral Shearing Interferometer

One important feature of a TWLSI is that it can be proved that the sum of the three phase gradients must be equal to zero, not counting the measurement noise.[5] Thus the noise amplitude can be estimated from the measurements themselves. This is obviously a better strategy for TWSLI's than for other types of interferometer in which the accuracy is extrapolated from measurements relative to some reference phases, since these reference phases are often tilts or defocus that are usually not representative of the phase defects to be analyzed in actual experiments.

Moreover, TWLSI sensitivity is easily adjusted by simple longitudinal translation of the observation plane, as described in Subsection 2.B. Last, the required phase gradients are derived simultaneously from a given image, and the recorded interferograms are optimally suited for a phase evaluation method based on Fourier transforms. All these features make this principle of interferometer attractive for low light level or real-time applications such as astronomical wave-front sensing. This is motivating the research on a new optical arrangement that deals with the major drawbacks of the current setup.

3. ACHROMATIZATION OF A THREE-WAVE LATERAL SHEARING INTERFEROMETER

In most low light level applications the aberrations analyzed are pure optical path differences, independent of wavelength. For example, in turbulent wave-front sensing, the atmosphere can be considered an achromatic medium in a first approximation. Better light efficiency can be achieved by an achromatic setup.

A. Grating Three-Wave Lateral Shearing Interferometer

Lateral shearing interferometers are achromatized by division of the analyzed wave front with gratings.[1–4] Interferograms are sensitive to the phase and not to the optical path differences, which are the only invariant quantities with respect to the wavelength for the considered cases. As the phase is proportional to the optical path divided by the wavelength, the lateral shift must be proportional to the wavelength. Hence different setups have been proposed, based on monodirectional gratings.

In a TWLSI it is necessary to use a bidirectional grating, since lateral shifts must go in different directions. We can determine the optimal grating by considering that the analyzed wave front must be divided into three equal replicas. It must diffract only three orders. Its Fourier transform $\mathrm{FT}(G)$ can be expressed as

$$\mathrm{FT}(G)(\mathbf{u}) = \sum_{n=1}^{3}\delta(\mathbf{u} - \mathbf{u}_n), \quad (7)$$

where $\mathbf{u}_n$ are three vectors at 120°. An inverse Fourier transform of this expression leads to the amplitude of the grating:

$$G(\mathbf{x}) = \sum_{n=1}^{3}\exp(2i\pi\mathbf{u}_n\cdot\mathbf{x}). \quad (8)$$

Considering this last expression, we see that the optimal grating is not easy to reach. Hence the selection of the three well-balanced orders requires a specific optical adaptation.

B. New Replication Device

The new replication device is described in Fig. 4. This is a bidirectional hexagonal grating placed in the entrance pupil of an afocal system. At the real focus of the afocal system the diffracted orders appear as separated luminous dots arranged along a hexagonal grid. It is then possible to apply a mask centered on the zero order and to occult all but the first three orders placed at the vertices of an isosceles triangle. The holes in the mask are elongated, as the impacts of the diffracted orders are translated radially proportionally to the wavelength. The interference pattern recorded in the exit pupil of the

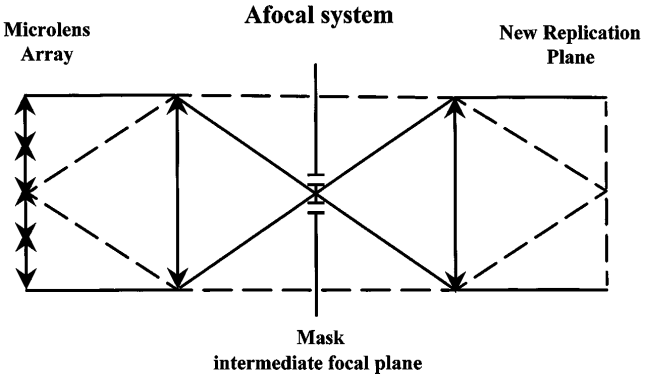

Fig. 4. New replication device.

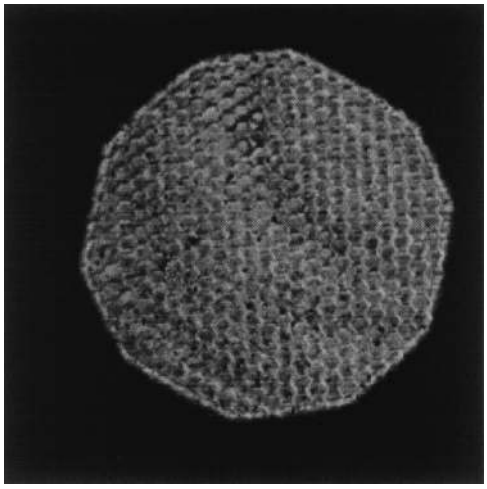

Fig. 5. Microlens array observed in the exit pupil of the afocal system.

afocal system corresponds to the desired three-wave interferogram. The exit pupil can thus be defined as the new replication plane.

Now the purpose is to find a grating that can be manufactured easily and that favors the three selected orders. It should be noticed that, as was the case in Subsection 2.C, a similar optical arrangement can be found for the generation of hexagonal arrays of microlenses by photoresist recording of three-beam interference.[6] In fact, the optical benches used in this technique are TWLSI's, and the defects in the recorded patterns can be explained by the same mathematical approach.

A microlens array is one of the rare bidirectional phase gratings that are in common use, which makes it a good candidate for the generation of diffracted orders. Its focal length must be adapted to maximize the energy efficiency in the three selected orders, which leads to a high f-number design. The maximum light efficiency with the use of a theoretical modeling, based on the fact that the distribution and the amplitudes of the different orders are found by the Fourier transform of the grating mesh, is estimated at 25% (8% for each order). This may be viewed as encouraging, since the mesh profile has not been optimized. That is, the central symmetry of a lenslet in no way contributes to the maximization of the energy in the three useful orders.

It should be noted that the bidirectional grating can also be obtained with the use of two crossed monodirectional gratings.

C. Experiments

We first constructed an optical bench to show the main characteristics of this new wave-front sensor concept. The setup consists of a hexagonal microlens array with a 0.2-mm pitch and a 14-mm focal length. The focal length was calculated to achieve the best light efficiency, approximately 0.6 μm. This array is placed in the entrance pupil of the afocal system, and a camera is aimed at the exit pupil. Different masks can be placed at the real focus of the afocal system.

If no mask is applied, the optical bench can be seen as a classical Hartmann–Shack wave-front sensor. The recorded interference patterns are shown in Figs. 5–7 for different longitudinal positions of the camera. If the camera is pointed at the exit pupil, almost no intensity variations are visible, as the microlens arrays are pure phase gratings. If it is pointed at the microlens focus, the interference pattern becomes the classical array of spots. If it is pointed at any other observation plane, different interference patterns can be observed, such as the one shown in Fig. 7.

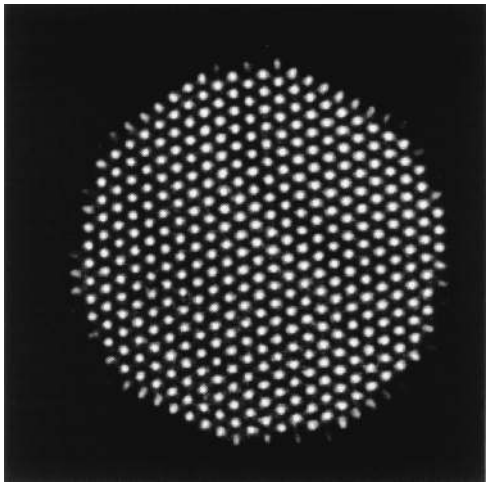

Fig. 6. Microlens array observed in the microlens focal plane.

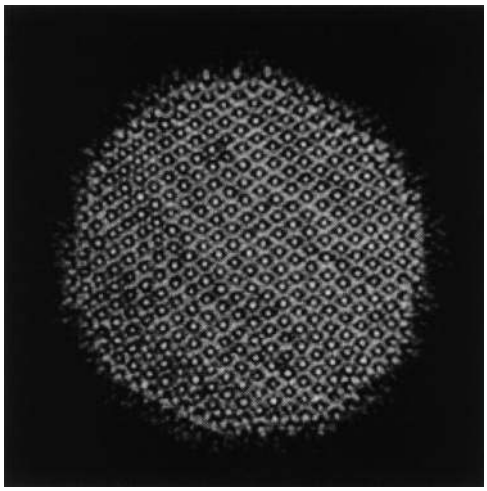

Fig. 7. Microlens array observed in an extrafocal plane.

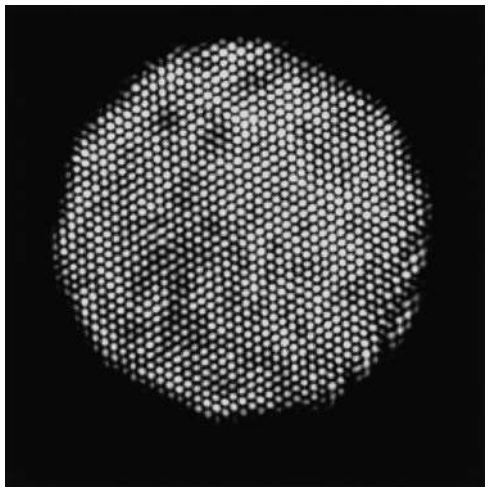

Fig. 8. Three-wave interferogram observed in the exit pupil of the afocal system.

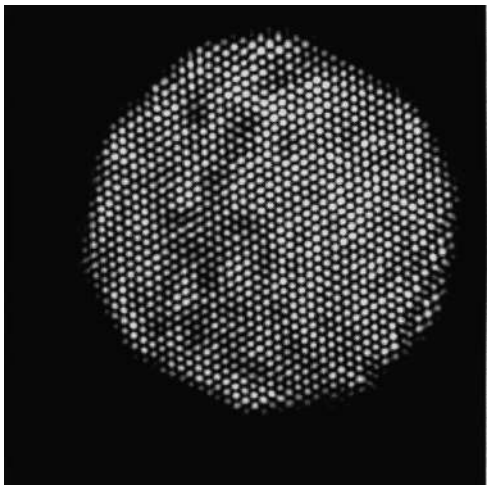

Fig. 9. Three-wave interferogram observed in the above-defined microlens focal plane (see Fig. 6). Note the similarity with Fig. 8 but for the blurred outline.

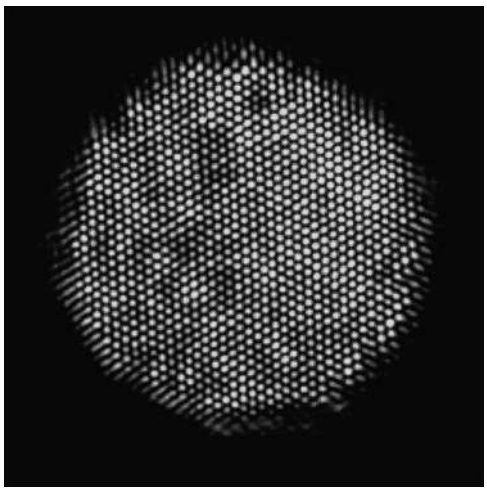

Fig. 10. Six-wave interferogram observed in the above-defined extrafocal plane (see Fig. 7). Note the similarity with Figs. 8 and 9; blur of the outline is now important.

Now a mask of three elliptical holes is placed at the intermediate focus. The basic Hartmann–Shack wavefront sensor then becomes a TWLSI, and three-beam interference patterns are observed. Figures 8–10 show the recorded images for the three above-mentioned longitudinal positions of the camera. The intensity pattern is obviously invariant, so that the only way in which one can evaluate the camera translation is to observe the blurred edge. Note also that the pitch of the interference pattern is divided by 2. This is due to the fact that the masking has increased the minimal distance between orders by a factor of 2.

One last experiment was conducted. This consisted of applying an annular mask that selects the first six orders. As the associated wave vectors also define a circle, the recorded patterns will behave in the same way as three-beam interference patterns (see Figs. 11–13). Note that the original pitch now returns.

This six-wave lateral shearing interferometer (SWLSI) offers two main advantages. First, an annular mask is easier to adjust than a three-hole mask. Second, the usable light efficiency is twice as good: 50%. On the other hand, the interference pattern is more complicated, and its Fourier transform contains many harmonics.

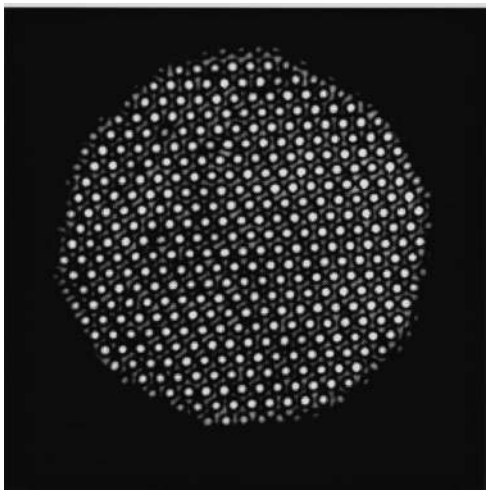

Fig. 11. Six-wave interferogram observed in the exit pupil of the afocal system.

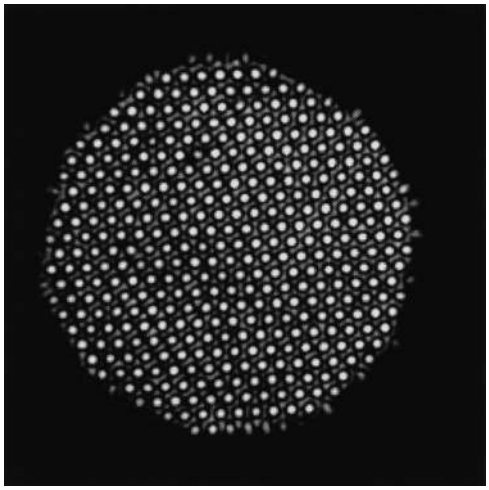

Fig. 12. Six-wave interferogram observed in the above-defined microlens focal plane (see Fig. 6).

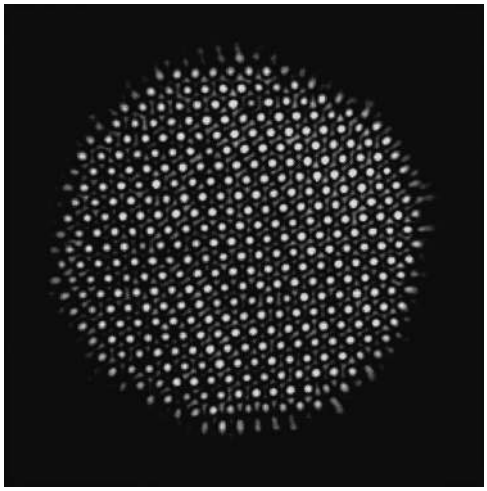

Fig. 13. Six-wave interferogram observed in the above-defined extrafocal plane (see Fig. 7).

D. Infinite Talbot Length Grating Interferometers

A periodic grating illuminated by a coherent plane wave diffracts many plane waves at different angles. If the interference pattern of these diffracted orders is observed at different longitudinal positions, the global irradiance changes. In fact, relative delays of the different plane waves are proportional to the diffraction angle. However, the original figure, observed in the grating plane, will be reproduced at periodic longitudinal locations. This phenomenon is called the Talbot effect and is associated with a characteristic Talbot length.

Here we have presented grating interferometers with three or six plane waves for which the delays vary simultaneously. The associated Talbot length is then equal to infinity, so that the irradiance remains the same. This property leads to the possibility of continuously adapting the sensitivity of these LSI's and thereby to the definition of a new class of grating interferometers with infinite Talbot length.

Note that it is also possible to define a four-wave setup if the hexagonal grating is replaced by a square one. Hence this family includes two-, three-, four-, and six-wave interferometers.

4. HARTMANN TESTS AND LATERAL SHEARING INTERFEROMETERS

Mainly two families of wave-front sensors are used in adaptive or active optics control. The first is that of LSI's, and the second is based on the Hartmann test.

The basic principle of the latter technique consists of putting a mask with holes in the pupil. Each hole is considered to emit a ray of light. The ray impacts are then recorded in a plane close to the focal plane. With perfect optics the recorded impacts will reproduce the original mask, with a global scaling effect. If aberrations are present, the impacts are displaced, as the rays are deviated from their ideal direction of propagation. These displacements are proportional to the slopes of the local wave front, as was the case for LSI's. The main improvement in this technique was proposed by Shack,[10] who replaced the mask of holes by a lenslet array, which led to better light efficiency.

Probably inspired by the fact that these two classes of wave-front sensors measure the same quantity, Roddier unified them.[11] To do this, he proposed a new description of the Hartmann test in which the usual mask of holes is considered as an order-diffracting grating. This leads to the LSI classical approach.

In this paper we have described achromatized TWLSI's as a special setup belonging to the LSI family. However, the practical application that we have proposed is close to the Hartmann–Shack wave-front sensor. It is in fact strictly identical if we remove the mask that selects the diffracted orders at infinity and allows the translational longitudinal invariance of the interference pattern. So it is possible to describe achromatized TWLSI's as a variant of the Hartmann–Shack wave-front sensor, which is experimental proof of how much these two widespread classes of wave-front sensors have in common.

5. CONCLUSION

The TWLSI is a new concept in lateral shearing interferometry that exhibits interesting properties for low light level wave-front sensing applications. One of these advantages is that the sensitivity can be adjusted by simple translation of a camera. Moreover, the generated interferograms are easily processed by Fourier transform techniques, and the error can be estimated from the measurements themselves.

This paper explains the design of new setups having good usable light efficiency for specific applications, in which the aberrated medium to be analyzed can be considered as achromatic. This was done by a special technique based on diffracted-order selection by bidirectional gratings. In the course of this work a new class of interferometers has been developed that involves more than two waves but preserves the longitudinal invariance of the interferogram modulation. In light of this remarkable property, they can be assembled in a class of their own, which we suggest should be called infinite Talbot length grating interferometers.

Achromatization of TWLSI's leads to new optical setups that are close to that of the Hartmann–Shack wave-front sensor. Compared with the characteristics of the classical system, the only new feature of the described setup is that it filters the orders diffracted by the microlens array at infinity. So achromatized TWLSI's (or SWLSI's) can be described as an interferometric setup belonging to the LSI class or as a variant of the Hartmann–Shack wave-front sensor. Because of this choice of description, the TWLSI can be viewed as a link between these two classes of wave-front sensors and as experimental proof of their unity.

ACKNOWLEDGMENTS

The authors thank C. Poinsot and Ph. Roze for their helpful contributions in carrying out the experiments. Thanks also go to B. Rosier, J. Deschamps, and V. Michau for their interest in this work.

REFERENCES

1. V. Ronchi, "Forty years of history of a grating interferometer," Appl. Opt. **3,** 437–451 (1967).

2. J. C. Wyant, "White light extended source shearing interferometer," Appl. Opt. **13,** 200–202 (1974),
3. C. L. Koliopoulos, "Radial grating lateral shear heterodyne interferometer," Appl. Opt. **19,** 1523–1528 (1980).
4. J. Schwider, "Continuous lateral shearing interferometer," Appl. Opt. **23,** 4403–4409 (1984).
5. J. Primot, "Three-wave lateral shearing interferometer," Appl. Opt. **32,** 6242–6249 (1993).
6. M. C. Hutley, "Optical techniques for the generation of microlens arrays," J. Mod. Opt. **37,** 253–265 (1990).
7. F. Roddier, "Wavefront sensing and the irradiance transport equation," Appl. Opt. **29,** 1402–1404 (1990).
8. K. Ichikawa, A. Lohmann, and M. Tadeka, "Phase retrieval based on the irradiance transport equation and the Fourier transform method: experiments," Appl. Opt. **27,** 3433–3436 (1988).
9. N. Streibl, "Phase imaging by the transport equation of intensity," Opt. Commun. **49,** 6–9 (1984)
10. J. C. Wyant and C. L. Koliopoulos, "Phase measurement systems for adaptive optics," AGARD Conf. Proc. No. 300, *Special Topics in Optical Propagation* (1981), Ref. 48, pp. 48-1–48-12.
11. F. Roddier, "Variations on a Hartmann theme," Opt. Eng. **29,** 1239–1242 (1990).